nature physics

LETTERS

https://doi.org/10.1038/s41567-018-0209-6

Superlight inverse Doppler effect

Xihang Shi[1,6], Xiao Lin[1,6*], Ido Kaminer[2*], Fei Gao[1,3], Zhaoju Yang[1,2], John D. Joannopoulos[4], Marin Soljačić[4] and Baile Zhang[1,5*]

It has long been thought[1] that the inverse Doppler frequency shift of light[2–13] is impossible in homogeneous systems with a positive refractive index. Here we break this long-held tenet by predicting a previously unconsidered Doppler effect of light inside a radiation cone, the so-called Vavilov–Cherenkov cone, under specific circumstances. It has been known from the classic work of Ginzburg and Frank that a superlight (that is, superluminal) normal Doppler effect[14–18] appears inside the Vavilov–Cherenkov cone if the velocity of the source v is larger than the phase velocity of light v_p. By further developing their theory, we discover that an inverse Doppler frequency shift will arise if $v > 2v_p$. We denote this as the superlight inverse Doppler effect. Moreover, we show that the superlight inverse Doppler effect can be spatially separated from the other Doppler effects by using highly squeezed polaritons (such as graphene plasmons), which may facilitate the experimental observation.

The Doppler effect, as a well-known phenomenon of motion-induced frequency shift, is one of the most fundamental mechanisms in physics and has vast applications in fields as varied as weather and aircraft radars, satellite global positioning systems, blood flow measurement in fetal vessels, laser vibrometry and the detection of extrasolar planets[1]. It occurs whenever the source and the observer move relative to each other. For the conventional Doppler frequency shift, the received frequency is higher (lower) compared to the emitted frequency during the approach (recession). In 1843, Christian Doppler propounded the conventional Doppler effect, first in relation to sound, and then to light[1]. Since then, it is believed that the counter-intuitive inverse Doppler frequency shift of light, where the sign of the frequency shift is opposite to that of the conventional Doppler frequency shift, cannot occur in homogeneous systems with a positive refractive index. In 1968, Victor Veselago predicted the inverse Doppler effect (with the inverse Doppler frequency shift) in homogeneous systems with a negative refractive index[2–6], for their capability of hosting the unusual waves (including surface plasmons) whose phase and group velocities are antiparallel. Moreover, the inverse Doppler effect has been predicted and demonstrated in new scenarios that rely on strongly inhomogeneous systems (without a negative refractive index), using various periodic structures[7–9] and interactions with shock waves[10–13].

Here we find that it is possible to create the inverse Doppler frequency shift inside the Vavilov–Cherenkov cone in homogeneous systems with a positive refractive index, as long as the radiation source moves with a velocity v larger than twice the phase velocity v_p of light; that is, $v > 2v_p$. We denote this new phenomenon as the superlight inverse Doppler effect, which breaks the above century-old belief. The superlight inverse Doppler effect is different from the superlight normal Doppler effect[14–18], which, first studied by Ginzburg and Frank in 1947, emerges when $v > v_p$. While Ginzburg and Frank's theory predicted that the frequency of the emitted photons transits from positive to negative when crossing the Vavilov–Cherenkov cone, we reveal that the Doppler effects inside the Vavilov–Cherenkov cone can be divided into two categories: the superlight normal and superlight inverse Doppler effects. The predicted superlight inverse Doppler effect circumvents the requirement for a negative-index homogeneous system or an inhomogeneous system, to create the inverse Doppler frequency shift. Moreover, Ginzburg and Frank's theory focused on the sign of change in the internal energy of the source during its radiation; in particular, the change in the internal energy of the source is positive (negative) inside (outside) the Vavilov–Cherenkov cone. We find that the change in the internal energy of the source, when larger (smaller) than the energy of the emitted photon, leads to the superlight inverse (superlight normal) Doppler effect. This also indicates that the major part of the change in the kinetic energy of the source turns into a positive increase in the internal energy of the source (the energy of the emitted photon) for the superlight inverse (superlight normal) Doppler effect. Therefore, our finding further develops Ginzburg and Frank's theory of the superlight normal Doppler effect.

For conceptual demonstration, we begin with the derivation of various Doppler effects of light. Consider that a radiation source (such as a point source with a dipole moment of $\overline{P}(\overline{r}', t') = \mathrm{Re}\{\hat{x}\, e^{-i\omega_0 t'}\}\delta(\overline{r}')$) moves in a system with a positive refractive index n ($n > 0$) and has a natural angular frequency of ω_0 ($\omega_0 > 0$) in the moving source frame. After applying the plane-wave expansion[19], the frequency and wavevector in the two different frames (that is, the laboratory frame and the moving source frame) can be directly linked through the Lorentz transformation; that is,

$$\begin{bmatrix} \overline{k} \\ \omega/c \end{bmatrix} = \begin{bmatrix} \overline{\overline{\alpha}} & +\gamma\overline{\beta} \\ +\gamma\overline{\beta} & \gamma \end{bmatrix} \begin{bmatrix} \overline{k}' \\ \omega'/c \end{bmatrix} \tag{1}$$

In equation (1), $\overline{k} = \hat{x}k_x + \hat{y}k_y + \hat{z}k_z$ ($\overline{k}' = \hat{x}k_x' + \hat{y}k_y' + \hat{z}k_z'$) and ω ($\omega' = \omega_0$) are the wavevector and the frequency in the laboratory frame (the moving source frame), respectively; $\overline{v} = +\hat{z}v$ is the velocity of the source, with its normalized form being $\overline{\beta} = \overline{v}/c$; $\gamma = (1-\beta^2)^{-1/2}$ is the Lorentz factor; finally, we use the definition $\overline{\overline{\alpha}} = \overline{\overline{I}} + (\gamma - 1)\frac{\overline{\beta}\,\overline{\beta}}{\beta^2}$, with $\overline{\overline{I}}$ being the unity dyad. From the Lorentz transformation,

[1]Division of Physics and Applied Physics, School of Physical and Mathematical Sciences, Nanyang Technological University, Singapore, Singapore. [2]Department of Electrical Engineering, Technion-Israel Institute of Technology, Haifa, Israel. [3]College of Information Science and Electronic Engineering, Zhejiang University, Hangzhou, China. [4]Department of Physics, Massachusetts Institute of Technology, Cambridge, MA, USA. [5]Centre for Disruptive Photonic Technologies, Nanyang Technological University, Singapore, Singapore. [6]These authors contributed equally: Xihang Shi, Xiao Lin.
*e-mail: xiaolinbnwj@ntu.edu.sg; kaminer@technion.ac.il; blzhang@ntu.edu.sg

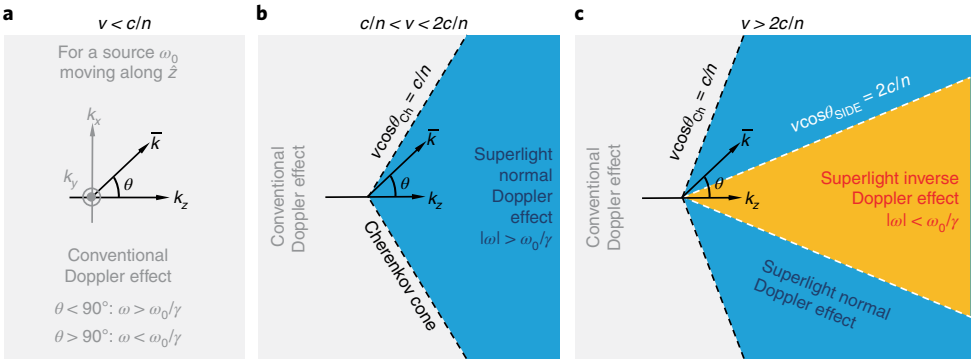

Fig. 1 | Representation in *k* space of the conventional Doppler effect, superlight normal Doppler effect and superlight inverse Doppler effect. A radiation source moves with a velocity of $\overline{v}$ along the $\hat{z}$ direction in a homogeneous system with a constant refractive index n ($n>0$). **a**, Only the conventional Doppler effect exists when $v<c/n$. **b**, When $v>c/n$, there is only the superlight normal Doppler effect inside the Vavilov–Cherenkov cone. **c**, When $v>2c/n$, the superlight inverse Doppler effect also appears inside the Vavilov–Cherenkov cone. In the source static frame, the source has a natural frequency ω_0. In the observer static frame, the received radiation fields have a frequency ω and a wavevector $\overline{k}$, where θ is the angle between $\overline{k}$ and the k_z axis (or $\overline{v}$). γ is the Lorentz factor. The angles of θ_{Ch} and θ_{SIDE} are the opening angles of the Vavilov–Cherenkov cone and of the cone in which the superlight inverse Doppler effect occurs, respectively. The value of $|\omega|$ goes to infinity at the angle of θ_{Ch}, and is equal to ω_0/γ at the angle of θ_{SIDE} (that is, no Doppler shift).

$$\omega=\gamma\omega_0+\gamma v k_z' \tag{2}$$

$$k_z=\gamma\frac{v}{c}\frac{\omega_0}{c}+\gamma k_z' \tag{3}$$

In equation (2), $k_z'\in(-\infty,+\infty)$, and the positive (negative) value of k_z' represents the generated waves propagating along the $+\hat{z}$ ($-\hat{z}$) direction in the source static frame. Since $\omega-\gamma\omega_0$ is proportional to k_z', one also has $\omega\in(-\infty,+\infty)$, and has $\omega<0$ ($\omega>0$) when $k_z'<-\omega_0/v$ ($k_z'>-\omega_0/v$). By combining equations (2) and (3), $k_z=\frac{\omega-\omega_0/\gamma}{v}$ is derived. With the knowledge of $k_z=n\frac{\omega}{c}\cos\theta$, where θ is the angle between the velocity of the source and the wavevector $\overline{k}$ of the emitted photon (see Fig. 1), one can further express various Doppler effects of light in the following ordinary way

$$n\frac{v}{c}\omega\cos\theta=\omega-\omega_0/\gamma \tag{4}$$

It is worth noting that the derivation of Doppler effects here, starting from equation (4), applies only to systems with a positive refractive index (that is, the group and phase velocities of waves are parallel or collinear). When $n\frac{v}{c}\cos\theta=1$, equation (4) is valid only if $\omega_0=0$. This corresponds to the well-known Vavilov–Cherenkov radiation[15,16], where the Vavilov–Cherenkov cone is denoted in Fig. 1. When $n\frac{v}{c}\cos\theta\neq1$, one has

$$\omega=\frac{\omega_0/\gamma}{1-n\frac{v}{c}\cos\theta} \tag{5}$$

Three types of Doppler effect can be distinguished from equation (5), where the crucial factor is the ratio between the velocity of the source and the z-component of the phase velocity ($v_p=c/n$) of light; that is, $n\frac{v}{c}\cos\theta$.

For type 1, when $n\frac{v}{c}\cos\theta<1$, equation (5) is satisfied only for $\omega>0$. When the source moves towards (away from) the observer (that is, $\theta<90°$ ($\theta>90°$)), one has $\omega>\omega_0/\gamma$ ($\omega<\omega_0/\gamma$), where the appearance of γ is due to the time dilation. This corresponds to the conventional Doppler effect of light (see Fig. 1a).

When $n\frac{v}{c}\cos\theta>1$, equation (5) is satisfied only for $\omega<0$. As emphasized in Ginzburg and Frank's theory[14–17], both frequencies ω_0 and ω are positive (see Type 1) if the source passes from an upper energy level to a lower one during the process of emission; that is, the energy $\hbar\omega$ of the emitted photon is supplied from both the internal energy of the source and its kinetic energy. However, ω_0 and ω are of opposite signs (see equations (6) and (7)) if the source becomes excited by passing from a lower energy level to an upper one during the emission process; that is, the kinetic energy of the source supplies both the energy of the emitted photon $\hbar|\omega|$ and the positive increase of the internal energy of the source. A similar transition between positive frequency and negative frequency may result in other interesting phenomena[20–23], including negative refraction[20], quantum friction[22], optical instabilities and spontaneous light emission by polarizable moving matter[23].

For type 2, when $2>n\frac{v}{c}\cos\theta>1$, from equation (5), one has

$$|\omega|=\frac{\omega_0/\gamma}{n\frac{v}{c}\cos\theta-1}>\omega_0/\gamma,\quad 2>n\frac{v}{c}\cos\theta>1 \tag{6}$$

This is in accordance with Ginzburg and Frank's theory[14–16] of the superlight normal Doppler effect (see Fig. 1b). If the dispersion of refractive index n is neglected, the frequency ω of emitted photons diverges and transits from positive infinity to negative infinity when crossing the Vavilov–Cherenkov cone. As a result of this, the superlight normal Doppler effect is also denoted as the anomalous Doppler effect in the literature[17,18]. Moreover, when $n\frac{v}{c}\cos\theta=2$, equation (5) leads simply to $|\omega|=\omega_0/\gamma$ (that is, no Doppler frequency shift).

For type 3, when $n\frac{v}{c}\cos\theta>2$, from equation (5), one has

$$|\omega|=\frac{\omega_0/\gamma}{n\frac{v}{c}\cos\theta-1}<\omega_0/\gamma,\quad n\frac{v}{c}\cos\theta>2 \tag{7}$$

This corresponds to the superlight inverse Doppler effect (see Fig. 1c) and the value of $|\omega|$ increases with the value of θ. The superlight inverse Doppler effect in equation (7) is different from the superlight normal Doppler effect in equation (6): in terms of Doppler-type frequency shifts, the former has $\Delta\omega=|\omega|-\omega_0/\gamma<0$ (that is, $|\omega|<\omega_0/\gamma$), while the latter has $\Delta\omega>0$ (that is, $|\omega|>\omega_0/\gamma$); in terms of energy–momentum conservation, the positive increase in the internal energy of the source is larger (smaller) than the energy

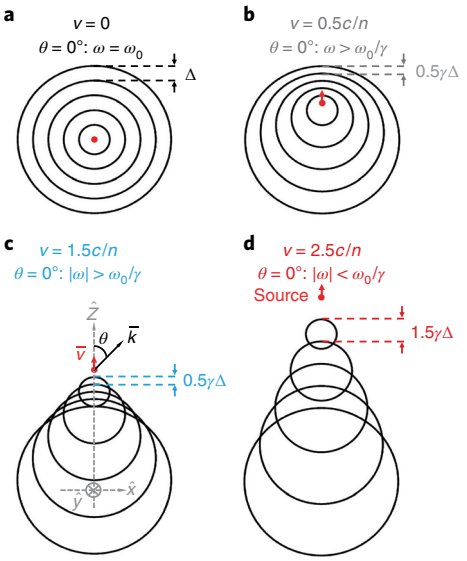

Fig. 2 | Real-space schematic demonstration of various Doppler effects of light. The radiation source (represented by the red dot) moves along the $\hat{z}$ direction in a homogeneous system with a constant positive refractive index ($n>2.5$ for illustration). The multiple phase fronts, illustrated by circular lines, are equally distributed in time. θ is the angle between $\overline{k}$ and $\hat{z}$ (or $\overline{v}$); when $\theta=0°$, $\overline{k}$ and $\hat{z}$ are in the same direction. **a**, When $v=0$, there is no Doppler effect. **b**, When $v<c/n$, the conventional Doppler effect exists at $\theta=0°$. **c**, When $c/n<v<2c/n$, the superlight normal Doppler effect appears at $\theta=0°$. When $v<2c/n$, the distance between successive wavefronts at $\theta=0°$ (labelled in each panel) is reduced and the waves bunch together. This leads to $|\omega|>\omega_0/\gamma$ at $\theta=0°$ in **b**,**c**. **d**, When $v>2c/n$, the distance between successive wavefronts at $\theta=0°$ is enlarged and the waves spread out. This leads to the superlight inverse Doppler effect ($|\omega|<\omega_0/\gamma$) at $\theta=0°$ in **d**. The Lorentz factor γ is different in each panel.

of the emitted photon for the superlight inverse (superlight normal) Doppler effect (see Methods); this indicates that the major part of the change in the kinetic energy of the source turns into the positive increase in the internal energy of the source (the energy of the emitted photon) for the superlight inverse (superlight normal) Doppler effect. Therefore, equations (6) and (7) describe two different types of Doppler frequency shift inside the Vavilov–Cherenkov cone. The superlight inverse Doppler effect is a new Doppler phenomenon of light that has never been discussed before.

From equation (7), the occurrence condition for the superlight inverse Doppler effect is $v>2c/n$. We note that this condition is numerically similar to the threshold for quantum friction between two uncharged polarizable moving slabs—that is, $|v_1-v_2|>c\left(\frac{1}{n_1}+\frac{1}{n_2}\right)$ (see equation (20) in ref. [22]), where v_1 (n_1) and v_2 (n_2) are the moving velocities (the refractive indices) of the two slabs; especially when $n_1=n_2=n$, one has $|v_1-v_2|>2c/n$. In addition, since the condition of $n\frac{v}{c}\cos\theta>1$ is possible only for $\theta<90°$, one always has $\theta<90°$ for the superlight normal and superlight inverse Doppler effects (see Fig. 1).

Figure 2 schematically shows the difference between the different Doppler effects in the time domain, marking multiple wavefronts that are equally distributed in phase. In the forward direction ($\theta=0°$; that is, $\overline{k}$ and $\overline{v}$ are in the same direction), both the conventional and superlight normal Doppler effects (that is, when $v<2c/n$) have the distance between successive wavefronts reduced, so the waves bunch together (Fig. 2b,c); in contrast, the superlight inverse Doppler effect (that is, when $v>2c/n$) has the distance between successive wavefronts enlarged, so the waves spread out (Fig. 2d). This shows a clear difference between the superlight inverse Doppler effect and the other two Doppler effects. Figure 2 also highlights a clear difference between the conventional Doppler effect and the two superlight Doppler effects: at $\theta=0°$, for the conventional Doppler effect (that is, when $v<c/n$), the observer first receives the wavefront emitted at an earlier time (Fig. 2b); however, for the superlight normal and superlight inverse Doppler effects (that is, when $v>c/n$), the observer first receives the wavefront emitted at a later time (Fig. 2c,d), corresponding to $\omega<0$ in equations (6) and (7).

Since the predicted superlight inverse Doppler effect requires two times the Cherenkov threshold (that is, $v>2c/n$), it is experimentally challenging to achieve for light waves. However, the high effective refractive index of highly squeezed polaritons (such as those in graphene)[24] may enable the superlight inverse Doppler effect to occur with a relatively small value of v. As an example, Fig. 3 uses the surface plasmon polaritons in graphene for conceptual demonstration. Assume that the source is a dipole with $\omega_0/2\pi=10$ THz, moving parallel to a graphene monolayer. The graphene has a chemical potential of 0.15 eV and a relaxation time of 0.3 ps. Then graphene plasmons have an effective refractive index $n=\frac{k_{spp}}{|\omega|/c}=19$ at $|\omega|/2\pi=10$ THz, where $\overline{k}_{spp}=\hat{x}k_x+\hat{z}k_z$ ($k_{spp}=|\overline{k}_{spp}|$) is the plasmonic wavevector parallel to the graphene plane. Using this wavevector, all of the Doppler effects for graphene plasmons can be described by a single equation (see Supplementary Information)

$$|\omega|\pm\omega_0/\gamma=k_{spp}v\cos\theta \tag{8}$$

where θ is the angle between $\overline{v}$ and $\overline{k}_{spp}$. When the minus (plus) sign is adopted, equation (8) characterizes the conventional (superlight normal and superlight inverse) Doppler effect of graphene plasmons, similar to equation (5) (equations (6) and (7)). When $v=0.1c$, one has $2v_{p0}>v>v_{p0}$ ($v_{p0}=c/n=c/19$), and thus there is only the conventional and superlight normal Doppler effects (see the dashed lines in Fig. 3). When $v=0.3c$, one has $v>2v_{p0}$; this way, the superlight inverse Doppler effect also emerges, as shown by the solid lines in Fig. 3 that cross between the two regimes.

The spatial overlap between the forward/backward-propagating graphene plasmons (both can have a smaller frequency than that of the source; see Fig. 2d) makes it difficult to detect the superlight inverse Doppler effect. Next we show in Fig. 4 that it is possible to convert the propagation of excited graphene plasmons from forward/backward to right/left, which can further facilitate potential experimental demonstrations in both the near field and far field (simply by introducing a scatter in the right region).

Consider a circularly polarized source, which moves along the $+\hat{z}$ direction and has a dipole moment of $\overline{P}(\overline{r}',t')=\mathrm{Re}\{(\hat{x}p_x+\hat{y}ip_y)e^{-i\omega_0t'}\}\delta(\overline{r}')$ with $p_x=p_y=1$ in the source static frame. Such circularly polarized sources with $v=0$ have been widely exploited for asymmetric excitation and can be formed by the interaction between the circularly polarized light and the designed defect[25]. Similarly, the circularly polarized moving dipole with $v\neq0$ (or with $v>0.1c$ in Fig. 4) can be effectively created by the interaction between a circularly polarized moving optical spot[26] and a designed defect (such as a long nanowire deposited above graphene, or a slit in the substrate of graphene); the optical spot moving with a tunable velocity, for example, can be achieved by illuminating the designed defect with an obliquely incident optical pulse, which is focused by a cylindrical lens to a line[26].

Figure 4a shows the distribution of the emitted plasmonic field in the graphene plane in the time domain; see the dynamics of the emitted plasmons in Supplementary Movie. When $v=0.3c$, two asymmetric caustics[27,28] are formed in the regions $x<0$ (the left side of the source) and $x>0$ (the right side of the source), respectively. Since the caustic frequency is close to the frequency of the wave component that dominates the plasmonic emission at each caustic[27],

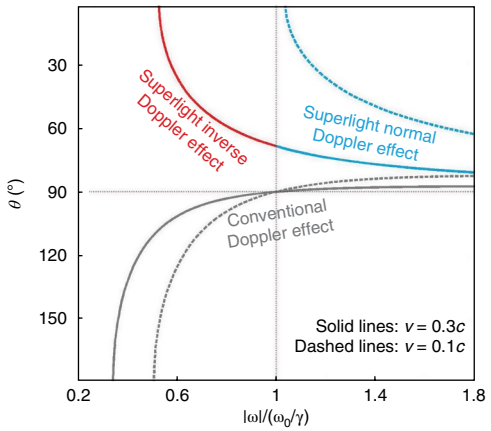

Fig. 3 | Superlight inverse Doppler effect of graphene plasmons. A dipole with $\omega_0/2\pi = 10$ THz moves parallel to a graphene monolayer surrounded by air. When $v = 0.1c$, only the conventional and superlight normal Doppler effects exist. When $v = 0.3c$, the superlight inverse Doppler effect also occurs. The chemical potential of graphene is 0.15 eV and the relaxation time is 0.3 ps. Here, and in the figure below, the frequency dispersion of graphene plasmons is considered and the effective refractive index of graphene plasmons is $n = 19$ at 10 THz. The superlight inverse Doppler effect thus appears only when $v > 2c/n = 2c/19$.

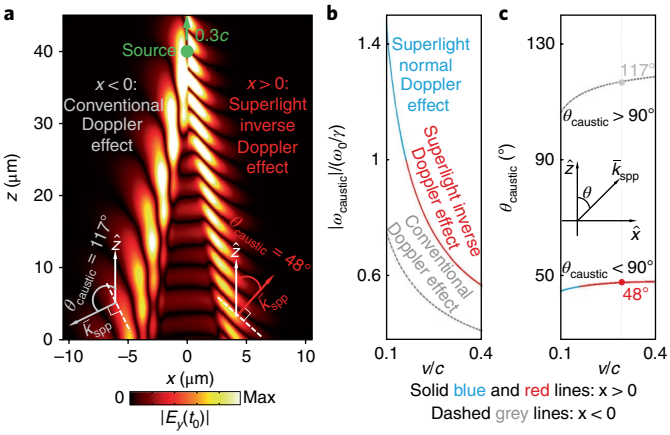

Fig. 4 | Real-space representation of the superlight inverse Doppler effect spatially separated from other Doppler effects. A circularly polarized dipole source with $\omega_0/2\pi = 10$ THz moves along the $+\hat{z}$ direction and parallel to the graphene monolayer. **a**, Distribution of the asymmetric radiation fields on the graphene plane with $v = 0.3c$ at the fixed time $t = t_0$ (when the source is at $z = 40$ μm). The excited plasmons propagate backwards in the region $x < 0$ (the left side of the source), while they propagate forwards in the region $x > 0$ (the right side); see the direction of the plasmonic wavevector $\overline{k}_{spp}$ in the inset. **b**, The two caustic frequencies $|\omega_{caustic}|$ as a function of v; these two frequencies dominate the plasmon emission in the regions $x < 0$ and $x > 0$, respectively. **c**, Propagation angles $\theta_{caustic}$; that is, the angle between $\overline{k}_{spp}$ and $\hat{z}$ (see inset) at each caustic frequency. For the case of $v = 0.3c$ in **a**, the corresponding $\theta_{caustic}$ is schematically illustrated along with the radiation fields in **a**. The region $x > 0$ is dominated by the superlight inverse Doppler effect when $v > 0.15c$ (see **a** for an example). The graphene (surrounded by air and parallel to the x–z plane) has a chemical potential of 0.15 eV and a relaxation time of 0.3 ps; the vertical distance between graphene and the source is 1 μm.

it can be used to determine the type of Doppler effect that dominates each region. Due to the asymmetry of the two caustics in Fig. 4a, regions $x < 0$ and $x > 0$ have different caustic frequencies. The caustic frequency is calculated from $\frac{d^2\varphi}{d\omega^2} = 0$ (ref. [27]), where $\varphi = k_x\frac{x}{t} + k_z\frac{z}{t} - \omega$ (see Supplementary Information).

Figure 4b,c shows the two caustic frequencies $|\omega_{caustic}|$ and the propagation angles $\theta_{caustic}$ (the angle between $\overline{k}_{spp}$ and $\overline{v}$ at each caustic frequency) for the regions $x < 0$ and $x > 0$ as a function of v, respectively. One can see that the region $x < 0$ is dominated by the conventional Doppler effect with $\omega_{caustic} < \omega_0/\gamma$, independent of the value of v. In contrast, the region $x > 0$ is dominated by the superlight normal Doppler effect with $|\omega_{caustic}| > \omega_0/\gamma$ when $v < 0.15c$, and, importantly, becomes dominated by the superlight inverse Doppler effect with $|\omega_{caustic}| < \omega_0/\gamma$ when $v > 0.15c$. It should be emphasized that, when $v > 0.15c$, the excited plasmon in region $x < 0$ (having the conventional Doppler effect) propagates along the backward ($-\hat{z}$) direction with $\theta_{caustic} > 90°$; in contrast, the excited plasmon in region $x > 0$ (dominated by the superlight inverse Doppler effect) propagates along the forward ($+\hat{z}$) direction with $\theta_{caustic} < 90°$ (see Fig. 4a and Supplementary Movie for an example).

Perhaps even more important is the vision our findings emphasizes: that the analogous phenomenon of the superlight inverse Doppler effect will exist in virtually any wave system in nature, including classical wave systems such as acoustic waves and surface waves, as well as quantum wave systems such as the Dirac equation; all of which have shown the occurrence of the Doppler effect, and therefore can now also support the analogous phenomenon of the superlight inverse Doppler effect. For example, the superlight normal Doppler effect has been used to construct the fibre-optical analogue of Hawking radiation[29,30]. It is thus intriguing to note the potential emergence of the superlight inverse Doppler effect in such a system, when the pulse (establishing an effective moving medium) moves with a velocity at least two times larger than the phase velocity of some ultraviolet modes[29].

Methods

Methods, including statements of data availability and any associated accession codes and references, are available at https://doi.org/10.1038/s41567-018-0209-6.

Received: 27 November 2017; Accepted: 12 June 2018;
Published online: 09 July 2018

References

1. Gill, T. P. *The Doppler Effect: An Introduction to the Theory of the Effect* (Logos, London, 1965).
2. Veselago, V. G. The electrodynamics of substances with simultaneously negative values of ϵ and μ. *Sov. Phys. Uspekhi* **10**, 509–514 (1968).
3. Leong, K., Lai, A. & Itoh, T. Demonstration of reverse Doppler effect using a left-handed transmission line. *Microw. Opt. Technol. Lett.* **48**, 545–547 (2006).
4. Chumak, A. V., Dhagat, P., Jander, A., Serga, A. A. & Hillebrands, B. Reverse Doppler effect of magnons with negative group velocity scattered from a moving Bragg grating. *Phys. Rev. B* **81**, 140404 (2010).
5. Chen, J. et al. Observation of the inverse Doppler effect in negative-index materials at optical frequencies. *Nat. Photon.* **5**, 239–242 (2011).
6. Lee, S. H., Park, C. M., Seo, Y. M. & Kim, C. K. Reversed Doppler effect in double negative metamaterials. *Phys. Rev. B* **81**, 241102(R) (2010).
7. Luo, C. Y., Ibanescu, M., Reed, E. J., Johnson, S. G. & Joannopoulos, J. D. Doppler radiation emitted by an oscillating dipole moving inside a photonic band-gap crystal. *Phys. Rev. Lett.* **96**, 043903 (2006).
8. Liu, W. F., Russell, P. St. J. & Dong, L. Acousto-optic superlattice modulator using a fiber Bragg grating. *Opt. Lett.* **22**, 1515–1517 (1997).
9. Hu, X. H., Hang, Z. H., Li, J. S., Zi, J. & Chan, C. T. Anomalous Doppler effects in phononic band gaps. *Phys. Rev. E* **73**, 015602 (2006).
10. Belyantsev, A. M. & Kozyrev, A. B. Reversed Doppler effect under reflection from a shock electromagnetic wave. *Tech. Phys.* **47**, 1477–1480 (2002).
11. Seddon, N. & Bearpark, T. Observation of the inverse Doppler effect. *Science* **302**, 1537–1540 (2003).
12. Reed, E. J., Soljacic, M. & Joannopoulos, J. D. Reversed Doppler effect in photonic crystals. *Phys. Rev. Lett.* **91**, 133901 (2003).
13. Reed, E. J., Soljacic, M., Ibanescu, M. & Joannopoulos, J. D. Comment on "Observation of the inverse Doppler effect". *Science* **305**, 778b (2004).
14. Ginzburg, V. L. & Frank, I. M. About Doppler effect at superlight velocity. *Dokl. Akad. Nauk SSSR* **56**, 583–586 (1947).

15. Frank, I. M. Optics of light sources moving in refractive media. *Science* **131**, 702–712 (1960).
16. Tamm, I. E. *Nobel Lectures, Physics 1942–1962* 470–482 (Elsevier, Amsterdam, 1964).
17. Ginzburg, V. L. Radiation by uniformly moving sources (Vavilov–Cherenkov effect, transition radiation, and other phenomena). *Phys.-Usp.* **39**, 973–982 (1996).
18. Einat, M. & Jerby, E. Normal and anomalous Doppler effects in a dielectric-loaded stripline cyclotron-resonance maser oscillator. *Phys. Rev. E* **56**, 5996–6001 (1997).
19. Lin, X. et al. Splashing transients of 2D plasmons launched by swift electrons. *Sci. Adv.* **3**, e1601192 (2017).
20. Pendry, J. B. Time reversal and negative refraction. *Science* **322**, 71–73 (2008).
21. Silveirinha, M. G. Quantization of the electromagnetic field in nondispersive polarizable moving media above the Cherenkov threshold. *Phys. Rev. A* **88**, 043846 (2013).
22. Silveirinha, M. G. Theory of quantum friction. *New J. Phys.* **16**, 063011 (2014).
23. Silveirinha, M. G. Optical instabilities and spontaneous light emission by polarizable moving matter. *Phys. Rev. X* **4**, 031013 (2014).
24. Lin, X. et al. All-angle negative refraction of highly squeezed plasmon and phonon polaritons in graphene-boron nitride heterostructures. *Proc. Natl Acad. Sci. USA* **114**, 6717–6721 (2017).
25. Bliokh, K. Y., Rodríguez-Fortuño, F. J., Nori, F. & Zayats, A. V. Spin–orbit interactions of light. *Nat. Photon.* **9**, 796–808 (2015).
26. Bakunov, M. I., Tsarev, M. V. & Hangyo, M. Cherenkov emission of terahertz surface plasmon polaritons from a superluminal optical spot on a structured metal surface. *Opt. Express* **17**, 9323–9329 (2009).
27. Shi, X. et al. Caustic graphene plasmons with Kelvin angle. *Phys. Rev. B* **92**, 081404(R) (2015).
28. García de Abajo, F. J. & Echenique, P. M. Wake potential in the vicinity of a surface. *Phys. Rev. B* **46**, 2663 (1992).
29. Philbin, T. G. et al. Fiber-optical analog of the event horizon. *Science* **319**, 1367–1370 (2008).
30. Bermudez, D. & Leonhardt, U. Hawking spectrum for a fiber-optical analog of the event horizon. *Phys. Rev. A* **93**, 053820 (2016).

Acknowledgements

This work was sponsored by the Singapore Ministry of Education (grant nos. MOE2015-T2-1-070, MOE2016-T3-1-006 and Tier 1 RG174/16 (S)), and the US Army Research Laboratory and the US Army Research Office through the Institute for Soldier Nanotechnologies (contract nos. W911NF-18-2-0048 and W911NF-13-D-0001). I.K. is an Azrieli Fellow, supported by the Azrieli Foundation, and was partially supported by the Seventh Framework Programme of the European Research Council (FP7-Marie Curie IOF) under grant no. 328853-MC-BSiCS.

Author contributions

All authors contributed extensively to the work presented in this paper. X.L., X.S. and B.Z. conceived the research. X.S. and X.L. performed the calculation. I.K., J.D.J., M.S, F.G., Z.Y. and B.Z. contributed insight and discussion on the results. X.L., X.S., B.Z., I.K., J.D.J. and M.S wrote the paper. B.Z., I.K., J.D.J. and M.S. supervised the project.

Competing interests

The authors declare no competing interests.

Additional information

Supplementary information is available for this paper at https://doi.org/10.1038/s41567-018-0209-6.

Reprints and permissions information is available at www.nature.com/reprints.

Correspondence and requests for materials should be addressed to X.L. or I.K. or B.Z.

Methods

Surface conductivity of graphene. The Drude model is adopted to characterize the surface conductivity of graphene in the studied frequency range of ~2–18 THz. The Drude model is sufficient, with no need to consider the nonlocal effect and the interband contribution, because the studied frequency range is far smaller than the frequency corresponding to twice the Fermi energy (that is, $2\mu_c = 0.3$ eV translates to ~72 THz; see Supplementary Information). We have considered the frequency dispersion of graphene plasmons for all of the results in Figs. 3 and 4.

Doppler effects of light derived from the conservation laws of energy and momentum. Here we derive the various Doppler effects from the conservation laws of energy and momentum. Consider that a radiation source (such as a dipole) has a natural angular frequency of ω_0 in the moving source frame and moves in a system with a positive refractive index n; this basic set-up is the same as that in the main text. When the momentum of the emitted photon $|\Delta\overline{p}| = n\hbar\omega/c$ is trivial in comparison with that of the source in the laboratory frame, the conservation law of momentum during radiation requires[14–17]

$$\Delta E = n\frac{v}{c}\hbar\omega\cos\theta \tag{9}$$

where θ is the angle between the velocity $\overline{v} = \hat{z}v$ of the source and the wavevector of the emitted photon (see Fig. 1), the change in the kinetic energy of the source is $\Delta E = \Delta\overline{\mathbf{p}}\cdot\overline{\mathbf{v}}$ and $\hbar$ is the reduced Planck constant. In the laboratory frame, ΔE is determined by the energy of the emitted photon $\hbar\omega$ and the change in the internal energy of the source $|\Delta U| = \hbar\omega_0/\gamma$ (refs [14–17]); that is,

$$\Delta E = \hbar\omega \pm \hbar\omega_0/\gamma \tag{10}$$

where $\gamma = (1-v^2/c^2)^{-1/2}$ is the Lorentz factor. In equation (10), as emphasized by Ginzburg and Frank[14–17], the minus sign should be adopted if the system passes from an upper energy level to a lower one during the radiation (that is, if the energy of the emitted photon is supplied from both the internal energy of the source and the kinetic energy); the plus sign should be used if, when emitting the photon, the system becomes excited (that is, if the kinetic energy supplies both the energy of the emitted photon and the positive increase in the internal energy of the source). From equations (9) and (10), one obtains

$$n\frac{v}{c}\omega\cos\theta = \omega \pm \omega_0/\gamma \tag{11}$$

To satisfy equation (11), the minus sign should be adopted when $n\frac{v}{c}\cos\theta < 1$ and the plus sign should be adopted when $n\frac{v}{c}\cos\theta > 1$. Namely, equation (11) is exactly the same as equation (4) in the main text.

In addition, from equation (11), the change in the internal energy of the source can be expressed as

$$|\Delta U| = \left|\hbar\omega\left(n\frac{v}{c}\cos\theta - 1\right)\right| \tag{12}$$

From equation (12) and the above analysis, the positive increase in the internal energy of the source is larger than the energy of the emitted photon for the case of $n\frac{v}{c}\cos\theta > 2$ (that is, leading to the superlight inverse Doppler effect), while is less than the energy of the emitted photon for the case of $1 < n\frac{v}{c}\cos\theta < 2$ (that is, leading to the superlight normal Doppler effect). This indicates that the major part of the change in the kinetic energy of the source turns into the positive increase in the internal energy of the source for the superlight inverse Doppler effect, and turns into the energy of the emitted photon for the superlight normal Doppler effect.

Reporting Summary. Further information on experimental design is available in the Nature Research Reporting Summary linked to this article.

Data availability. The data that support the plots within this paper and other findings of this study are available from the corresponding author upon reasonable request.